PHYSICAL REVIEW A VOLUME 43, NUMBER 12 15 JUNE 1991

Equilibrium budding and vesiculation in the curvature model of fluid lipid vesicles

Ling Miao, Bertrand Fourcade,* Madan Rao, and Michael Wortis
Department of Physics, Simon Fraser University, Burnaby, British Columbia, Canada V5A 1S6

R. K. P. Zia
Department of Physics and Center for Stochastic Processes in Science and Engineering, Virgina Polytechnic Institute and State University, Blacksburg, Virginia 24061-0435

(Received 7 November 1990)

According to a model introduced by Helfrich [Z. Naturforsch. **28c**, 693 (1973)], the shape of a closed lipid vesicle is determined by minimization of the total bending energy at fixed surface area and enclosed volume. We show that, in the appropriate regime, this model predicts both budding (the eruption of a satellite connected to the parent volume via a neck) and vesiculation (the special case when the neck radius goes to zero). Vesiculation occurs when the minimum is located at a boundary in the space of configurations. Successive vesiculations produce multiplets, in which the minimum-energy configuration consists of several bodies coexisting through infinitesimal necks. We study the sequence of shapes and shape transitions followed by a spherical vesicle of radius R_V, large on the scale R_0 set by the spontaneous curvature, as its area A increases at constant volume $V=4\pi R_V^3/3$. Such a vesicle periodically sheds excess area into a set of smaller spheres with radii comparable to R_0. We map out this (shape) phase diagram at large volume. In this region the phase diagram is dominated by multiplets and reflects the details of the shedding process. The overall effect of successive vesiculations is to reduce the energy from a quantity of order R_V^2 down to zero or near zero when the area reaches $3V/R_0$; however, the decrease is not uniform and the energy $E(A,V)$ is not convex.

I. INTRODUCTION

"Budding" and "vesiculation" refer to processes in which a single, more or less spherical vesicle (or cell in the biological context), when subjected to change in some external parameter or stimulus, undergoes a shape transformation to produce one or more globular appendages linked to the parent body through narrow necks or tubes. When the neck diameter is positive, we shall call the process "budding." To distinguish the limiting case where the neck diameter goes to zero (in a sense which will be made precise below), we shall refer to this as "vesiculation." Both these processes affect the shape but not the topology. If subsequently the appendage breaks off from the parent body (fission), only then does the topology change. In biological systems[1] such processes are usually driven by complex chemical stimuli and may result in the extrusion of interior material (or, for the inverse process, in the incorporation of exterior material). It is the thesis of this paper that budding and vesiculation can and do both occur as adiabatic processes (i.e., processes involving only equilibrium states) in the simplest model of fluid vesicles.[2]

The static shapes of closed fluid lipid-bilayer membranes with dimensions which are large on the molecular scale may be modeled by the energy functional,

$$E[c_1,c_2]=\frac{\kappa}{2}\int dS\,[c_1(\mathbf{r})+c_2(\mathbf{r})-c_0]^2\ , \tag{1}$$

which seems originally to have been introduced by Canham[3] and has subsequently been exploited by Helfrich and co-workers,[4,5] Evans and Skalak,[6] and many others.[7–9] In this expression c_1 and c_2 are the principal curvatures at each point $\mathbf{r}$ and the constant c_0 is twice the so-called spontaneous curvature. The integral is over the closed vesicle surface. For a two-dimensional vesicle embedded in three dimensions, the integral is dimensionless and the bending elastic constant κ sets the energy scale. A similar integral over the local Gaussian curvature c_1c_2 gives a contribution which, by the Gauss-Bonnet theorem, is independent of shape for a given topology and is omitted here, since we shall deal only with configurations of fixed (spherical) topology.

Regarded as a Landau functional, Eq. (1) contains all possible local, isotropic, and Euclidean invariant terms through second order in the curvature. Additional effects involving higher powers of the curvature and/or local curvature derivatives are not excluded by symmetry but enter only as correction terms for large vesicles.

The physical origin of the spontaneous curvature under given experimental conditions is a matter of present interest and even controversy. Nonzero values of c_0 may arise, for example, from chemical asymmetry between the interior and exterior of the membrane[10] or from different areas of the two leaves of the bilayer (the bilayer-couple mechanism).[11] Whether these mechanisms suffice to explain observed shapes is unclear. In any case, we must keep in mind that the "constant" c_0 may depend on both microscopic (chemical) and macroscopic (geometrical) variables. In what follows, we shall study a model system in which c_0 is taken to be constant. If under laboratory conditions c_0 turns out to depend on the surface area A

and/or volume V of the vesicle, then our phase diagrams remain applicable, but the paths of constant A and V will require suitable modification.

In what follows, we shall assume that the equilibrium vesicle shape is that which minimizes the energy (1) at given A and V, i.e., the mechanically stable shape. For many experimental systems (e.g., lecithins[12]) κ is appreciably larger than room temperature, so thermal fluctuations are small and this zero-temperature ($T=0$) approximation is reasonable. Under these conditions the energy scale drops out and only geometry is left. There remain three length scales R_A, R_V, and R_0, defined by $A=4\pi R_A^2$, $V=4\pi R_V^3/3$ (note that $R_A \geq R_V$), and $c_0=2/R_0$. We shall assume that $c_0 \neq 0$. There is then no loss of generality[13] in taking $c_0>0$, so spheres of radius R_0 (which we shall refer to as "Helfrich spheres") cost no energy, and we are free to set the scale of length by taking $c_0=1$ (i.e., $R_0=2$).

Minimizing Eq. (1) at fixed A and V leads to a catalog of shapes, which was first compiled by Deuling and Helfrich[5] and has subsequently been extended and refined by other authors.[7–9,11,14] For technical reasons this work has been restricted to axisymmetric shapes.[15] Furthermore, many (but not all[11,14]) authors have restricted their attention to the regime $R_A, R_V \sim 1$, i.e., vesicle dimensions comparable to R_0. Normal erythrocyte shapes[6,16] occur in this regime (with a negative value of c_0). A variety of shapes and shape transitions do, indeed, show up in this region, including discocytes, stomatocytes, torocytes, etc.; however, budding and vesiculation are absent.

The purpose of this work is twofold. First, we wish to explore the regime $R_A \sim R_V \gg 1$, of large and more or less full vesicles. In this we are motivated by the observations of Evans and Rawicz,[12] Sackmann, Duwe, and Engelhardt[17] and others[18,19] on artificial vesicles with sizes in the range of 20 μm. These vesicles start out approximately spherical. Heating leads to an area expansion which is much larger than the corresponding volume expansion, so the process may be idealized as area increase at constant volume ($k_B T$ remains always much less than κ, so $T=0$, effectively). Budding and vesiculation are observed. Our second focus is to construct for the above regime a real "phase diagram," showing the systematics of shapes and shape changes, rather than just a catalog of possible shapes. The idea here is that the minimum-energy shape changes smoothly as parameters are varied (single-phase regions), except along certain special surfaces (phase boundaries) in parameter space where abrupt shape transformations occur, sometimes but not always involving symmetry change. At these phase boundaries, the total energy is continuous, but its first derivative may change discontinuously (first-order transition) or continuously (second-order transition). Budding and vesiculation occur at two such phase transitions.

The physical origin of budding and vesiculation in the curvature model (1) is easy to understand. When $R_A=R_V$, the vesicle is a sphere. As area increases (or, equivalently, as volume decreases) an excess area ΔA becomes available. If we write $A=4\pi R_V^2(1+\Delta)$ in terms of the fractional excess area, then $\Delta A=4\pi R_V^2\Delta$. As soon as ΔA becomes comparable to $4\pi R_0^2$ (16π in our units), it becomes favorable to shed the excess area in the form of a bud with radius comparable to R_0, which costs very little energy (no energy when the radius is equal to R_0). As the area increases further, the shedding process continues in a more or less periodic manner until the volume of the parent body becomes, itself, comparable to that of the Helfrich sphere. The full sequence of shape transitions is quite complicated, and we shall find that it involves a nice interplay of some configurations with small necks (buds) and others in which the neck radius shrinks to zero[20] (vesiculation).

This mechanism for budding and vesiculation appears originally to have been proposed by Luke and Kaplan;[21] however, no systematic calculations were done until very recently. Vesiculated shapes appear naturally in the bilayer model[11] as purely geometrical limits, where the area difference is maximal; however, the energy functional in that model lacks the c_0 terms of Eq. (1) and energetic considerations are quite different. Two groups have recently studied these phenomena from a point of view similar to ours. Seifert and co-workers[14,18] have carried out a comprehensive study of the low-volume regime (i.e., $V \sim 4\pi R_0^2$). Budding and vesiculation do occur, but the sequences which we shall find at high volume are not present. Similarly, Wiese and Helfrich[22] find that a daughter vesicle is formed at low volume, but do not distinguish between budding[23] and vesiculation.

The plan of this paper is as follows. Section II introduces the minimization of the energy functional (1), the Euler equation to which it leads, and the resulting (shape) phase diagram. Section III treats vesiculation in a general way. Vesiculation occurs when the minimum-energy configuration lies at a boundary in the space of possible shapes, and it corresponds physically to a situation where the energy of a small neck decreases with the neck radius. Treatment of the mathematical bifurcation which occurs as the minimum approaches this boundary (i.e., as the equilibrium neck radius approaches zero) is deferred to a subsequent paper.[24] The members of the multiplet configurations formed by vesiculation must satisfy coexistence conditions. In Sec. IV, we collect a set of useful results for spherical and nearly spherical shapes. Section V presents numerical results for shape evolution at a volume ($V=272$ in dimensionless units), which is large enough to allow several vesiculations but still small enough to be amenable to numerical integration of the shape equations (which become increasingly unstable at high volume). In Sec. VI, we map out the full phase diagram (quasianalytically) for the regime of high volume and an area which is not too large ($A<3V/R_0$). Section VII concludes with a discussion of outstanding problems, including the relation of our results to experiment.

II. FORMULATION OF THE PROBLEM: EULER SHAPES AND PHASE DIAGRAMS

Following Deuling and Helfrich,[5] we incorporate the area and volume constraints on the energy minimization by introducing the variational functional

$$\Phi[S]=E[S]+\sigma A[S]-pV[S] , \tag{2}$$

which, in analogy with thermodynamics, we shall refer to as a free energy. σ and p are Lagrange multipliers,[25] S stands for the vesicle shape, and the square brackets denote functional dependence. Making (2) stationary subject to the condition of axial symmetry (which we shall assume throughout) leads to the Euler equation[26] originally derived by Helfrich,[4,5]

$$\frac{dc_m}{dr}+\frac{c_m-c_p}{r}=\frac{r}{2[1-(rc_p)^2]} \times\{c_p[(c_p-1)^2-c_m^2]+2\sigma c_p-p\}\ , \quad (3)$$

where we have chosen units such that κ and c_0 are equal to unity, and r is the distance to the axis. c_m and c_p are the principal curvatures, defined positive when the center of curvature lies along the direction of the interior normal $\hat{\mathbf{n}}$ (see Fig. 1). The plane of c_m contains the rotation axis and is perpendicular to that of c_p. Axial symmetry requires

$$\frac{dc_p}{dr}=\frac{c_m-c_p}{r}\ . \quad (4)$$

If z measures distance along the symmetry axis [so $z(r)$ represents the shape S] and Θ is the angle between the local tangent and the plane perpendicular to the symmetry axis, then

$$\frac{dz}{dr}=\tan\Theta\ , \quad (5)$$

and it is convenient to represent

$$c_p=\frac{\sin\Theta}{r},\quad c_m=\frac{d\sin\Theta}{dr}\ , \quad (6)$$

which incorporates Eq. (4).

In order that the vesicle shape S be smooth, appropriate boundary conditions must be applied at the singular points of Eq. (3). For example (see Fig. 1), near $r=0$ at the lower end of the vesicle

$$\sin\Theta(r)=\alpha_0 r+(\alpha_0-2\alpha_0^2+2\sigma\alpha_0-p)\frac{r^3}{16}+\cdots\ , \quad (7)$$

while near a belly of radius a

$$\sin\Theta(r)=1-\alpha_2 t^2\pm\alpha_3 t^3+\cdots\ , \quad (8)$$

where $t=\sqrt{r-a}$, and the upper (lower) signs of the odd terms apply below (above) the belly.

The parameter α_0 in Eq. (7) gives the curvature on the axis and must be set at one of some discrete set of initial values $\{\alpha_0^{(n)}\}$ in order that the computed Euler shape should close smoothly above. The corresponding shapes, which we denote $S_n(\sigma,p)$, have free energies $\Phi_n(\sigma,p)=\Phi[S_n(\sigma,p)]$ and corresponding areas $A_n(\sigma,p)$ and volumes $V_n(\sigma,p)$. Because $S_n(\sigma,p)$ makes $\Phi[S]$ stationary, it is easy to show that

$$\frac{\partial\Phi_n(\sigma,p)}{\partial\sigma}=A_n,\quad \frac{\partial\Phi_n(\sigma,p)}{\partial p}=-V_n\ . \quad (9)$$

Because there are typically many solutions to the Euler equation, the functions $\Phi_n(\sigma,p)$ form a family of sheets[27] over the (σ,p) plane. On a single sheet the dependence $\Phi_n(\sigma,p)$ is generally analytic; however, the sheets can cross, they can fold over and connect to each other, and they can merge into or bifurcate from one another.

If the free energy $\Phi_n(\sigma,p)$ is not convex, there may be several solutions to the inversion $A=A_n(\sigma,p)$, $V=V_n(\sigma,p)$ for each n. Let m label the complete set of such solutions (i.e., over both n and the different solutions for each fixed n). The corresponding family of energy surfaces $E_m(A,V)$ is also complex; however, local bifurcation structure is normally preserved in the change of variables.[28] It is a consequence of the Legendre-transform structure that

$$\frac{\partial E_m(A,V)}{\partial A}=-\sigma_m,\quad \frac{\partial E_m(A,V)}{\partial V}=p_m\ , \quad (10)$$

which is true as a local statement for any sheet m. Although Eqs. (9) and (10) look very "thermodynamic," it must be kept in mind that the functions $\Phi_n(\sigma,p)$ and $E_m(A,V)$ do not in general satisfy convexity conditions even locally, so second derivatives such as $\partial^2 E_m/\partial A^2$ and $\partial^2 E_m/\partial V^2$ may have either sign.

Once all the energy sheets are known (and we shall see in Sec. III that the Euler-shape sheets are only a subset), the solution to the constrained minimization problem originally posed is

$$E(A,V)=\min_s E[S]|_{A,V}=\min_m E_m(A,V)\ , \quad (11)$$

i.e., the solution always chooses the lowest-energy sheet at each point (A,V).[29] In regions (A,V) where the solution remains on a single sheet E_m, the energy $E(A,V)$ is analytic. Nonanalyticities arise when the solution passes from one sheet onto another. This occurs where sheets cross or where they merge, bifurcate, or terminate in some other way. The energy is continuous over the accessible region of the (A,V) plane;[30] however, as we shall

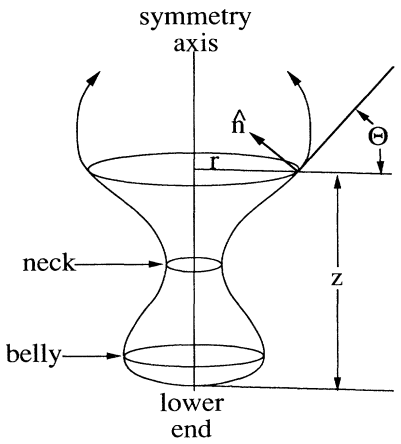

FIG. 1. Axisymmetric vesicle shapes. We start with some initial curvature α_0 at the lower end of the vesicle and integrate out through one or more extremal points. If α_0 has been correctly chosen, then the figure closes smoothly on the axis. The curvatures c_m and c_p are defined positive when the corresponding center of curvature lies along the line of the interior normal $\hat{\mathbf{n}}$.

see in some detail, it is not generally convex and its derivatives may be discontinuous. Borrowing the terminology of phase transitions, we call the regions of analyticity "single-phase" regions and refer to the loci of nonanalyticity as "phase boundaries." When $\partial E/\partial A$ and/or $\partial E/\partial V$ changes discontinuously, we refer to the transition as "first order" (generically, this is the situation when sheets cross); otherwise, it is "second order" (as occurs at bifurcations). The loci of nonanalyticity in (A,V) constitute the "(A,V) phase diagram." The corresponding loci in the (σ,p) plane constitute the "(σ,p) phase diagram." Note that crossing a first-order phase transition corresponds to a discontinuous jump in (σ,p) and may occur at a point where the surface $\Phi_n(\sigma,p)$ is smooth.

III. BOUNDARY MINIMA, COEXISTENCE, AND MULTIPLETS

It might seem that all minimum-energy shapes correspond to solutions of the Euler equation (3). To understand why this is not so, consider an arbitrary smooth function f of a single scalar variable x in the interval $[b,c]$. To find the minimum of f, it is true that we must search the points where $df/dx=0$ (analogous to the Euler equation); but, we must also compare with the boundary values $f(b)$ and $f(c)$. These "boundary" configurations correspond in the vesicle problem to configurations which consist of two or more Euler shapes which communicate (exchanging area and volume) via necks of arbitrarily small (but nonzero[31]) diameter [see Fig. 2(a)]. Technically, such a shape should be thought of as the limit of a single connected (topologically spherical) shape with one or more necks which approach zero diameter. At first sight it might appear that the large curvatures that occur near the necks would always lead to large energies in the Landau functional (1) and would place such configurations very far from any energy minimum. (Indeed, this is true for a $D=1$ vesicle in two space dimensions, and for this system vesiculation is absent). The key point is that, although the absolute values of the two curvatures diverge as the neck diameter a tends to zero, the signs are opposite. It turns out that, by an appropriate choice of neck shape, the energy of the neck region can be reduced so that it scales (linearly) as Ca, as a goes to zero. As long as the coefficient C is positive, the limiting configuration is locally an energy minimum and can compete with the lowest-energy Euler shape of the same area and volume. We shall call these limiting configurations, in which two or more Euler shapes touch tangentially and communicate via an infinitesimal neck, "multiplets."

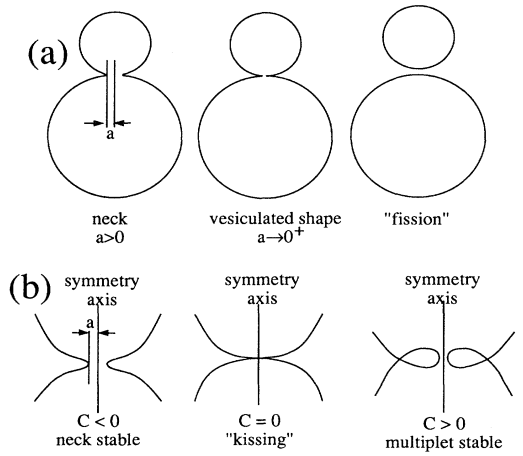

FIG. 2. Vesiculated shapes and the kissing condition. (a) Vesiculated shapes consist of two or more parts connected via infinitesimal necks. In situations where such shapes are stable (i.e., lowest energy), increasing the neck radius a from zero raises the energy ($C>0$). "Fission" changes the topology and is not considered here. (b) Sequence of Euler shapes corresponding to passage across a kissing boundary. On one side $C<0$, and the necked shape is stable; on the other the Euler shape is self-intersecting, $C>0$, and the multiplet is stable. At the bifurcation, the kissing condition $C=0$ is satisfied.

We defer detailed discussion of the neck region to a subsequent paper[24] and simply quote here the three results that are crucial to our discussion. We have shown (for axisymmetric shapes) the following:

(a) In the limit $a\rightarrow 0$, the energy of the neck region vanishes.

(b) The coefficient C is proportional to $1-1/R_1-1/R_2$, where R_1 and R_2 are the radii of curvature at the point of contact.[32] The multiplet is locally stable when this bracket is positive.

(c) Bifurcation between a budded or necked shape (with $a>0$) and a fully vesiculated shape ($a=0$) takes place when $C=0$ ("the kissing condition"). The kissing condition defines lines in the (σ,p) plane (see, e.g., Sec. IV and Fig. 3). Near such a line there are two sheets of similar stationary-energy shapes, one necked and one vesiculated [Fig. 2(b)]. The two sheets meet at the kissing boundary and their energy ordering interchanges. Thus, on one side of the kissing line, $C<0$ and the necked shapes have lower energy than the multiplet; while, on the other side, $C>0$ and the vesiculated shapes have lower energy. For C positive, the neck becomes self-intersecting and is an unacceptable shape for a real vesicle.

We now discuss the thermodynamics of the multiplet configurations. A multiplet consisting of $M(\geq 2)$ smooth shapes may be taken to satisfy the following conditions:

$$E(A,V)=\sum_{i=1}^{M} E_i(A_i,V_i) \tag{12}$$

and

$$A=\sum_{i=1}^{M} A_i, \quad V=\sum_{i=1}^{M} V_i\ , \tag{13}$$

where $i=1,\ldots,M$ labels the members of the multiplet. Notice that, in omitting any energy contribution due to the necks, we have made use of result (a) above. In looking for an energy minimum, there is no loss of generality in choosing multiplet members to be Euler shapes, since the lowest-energy *smooth* shape of given area and volume is an Euler shape. It remains to determine how to minimize the energy (12) by redistributing the area and volume among the members of the multiplet subject to

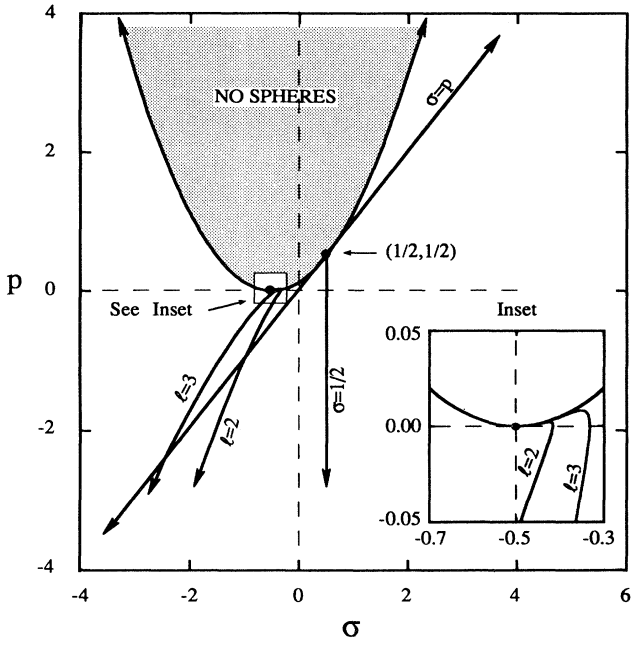

FIG. 3. The (σ,p) plane, showing special features associated with spherical shapes. In the interior of the parabola, Eq. (17), there are no spherical Euler shapes. Outside, there are two distinct spheres with radii given by Eq. (16). On the parabola, the radii of the two spheres become equal. The lines labeled $l=2$ and 3 mark the bifurcation boundaries, Eq. (23), at which spherical shapes become unstable to small shape perturbations of the corresponding spherical harmonics. Note in the inset how all these bifurcation lines emerge from the point $(-\frac{1}{2},0)$. Lowest-energy weakly deformed shapes lie to the right of these curves. $\sigma=p$ is the locus of Helfrich spheres ($R=2$), which automatically satisfy the kissing condition. $\sigma=\frac{1}{2}$ is the line along which the two (unequal) coexisting spheres have radii satisfying the kissing condition.

the constraints (13). Incorporating the constraints via Lagrange multipliers and using Eq. (10) for the individual multiplet members yields

$$\sigma_i=-\frac{\partial E_i}{\partial A_i}=\sigma,\quad p_i=\frac{\partial E_i}{\partial V_i}=p \tag{14}$$

as the conditions for stationarity.[33] Thus the coexistence condition for the members of a given multiplet is that they share values of σ and p. When all members of the multiplet satisfy $\partial^2 E_i/\partial A_i^2>0$ and $\partial^2 E_i/\partial V_i^2>0$, then the stationary point is guaranteed to be a local minimum.[34] If either second derivative is negative for all members of the multiplet, then the stationary point cannot be a local minimum.[35] In general, the signs are mixed and nothing can be said without specific calculation.

The stationary point or points given by (14) define a set of multiplet energy sheets $E_m(A,V)$ which must be combined with the Euler sheets of Sec. II before selecting the true lowest energy state (11) at each given point (A,V).

IV. SPHERES, THE SPHERICAL SHEET, AND LOCAL PERTURBATIONS

In the (A,V) plane, spheres lie along the line $V=A^{3/2}/3\sqrt{4\pi}$, which bounds the physical region. Each point on this line corresponds to a particular radius R. The spherical symmetry of the problem guarantees that such shapes will be solutions of the Euler problem and, indeed, we see that $c_m(r)=c_p(r)=1/R$ satisfies Eqs. (3) and (4) provided

$$p=\frac{2\sigma}{R}+\frac{1}{R}\left[1-\frac{2}{R}\right], \tag{15}$$

which is just the usual soap-bubble formula corrected for spontaneous curvature. Note that Eq. (15) is linear in both σ and p, so that each sphere is represented by a straight line in the (σ,p) plane.[36] Inverting Eq. (15) to find the allowed radii gives

$$\frac{1}{R}=\tfrac{1}{4}\{(1+2\sigma)\pm[(1+2\sigma)^2-8p]^{1/2}\}, \tag{16}$$

so that spheres are forbidden above

$$p=(1+2\sigma)^2/8. \tag{17}$$

Along this boundary (Fig. 3) the two allowed spheres have equal radius. In the region below this curve, there are two free-energy sheets $\Phi_n(\sigma,p)$ for spheres, which join smoothly along the boundary.

All this structure maps in the (A,V) plane onto the line $V=A^{3/2}/3\sqrt{4\pi}$ with corresponding energy

$$E(R)=E_0(R)=2\pi(2-R)^2. \tag{18}$$

The mechanism for this reduction is a simple property of the Legendre transform.[37] Consider the family of planes $P(\sigma,p;R)$ (parameterized by R) defined by $\Phi_0(R)=E_0(R)+4\pi R^2\sigma-4\pi R^3 p/3$. Note that, for each value of R, the entire plane $P(\sigma,p;R)$ maps under Legendre transform into the single point $(4\pi R^2,4\pi R^3/3)$ in the (A,V) plane. Now, the intersection of the spherical sheet $\Phi_{\text{sphere}}(\sigma,p)$ with the plane $P(\sigma,p;R)$ lies along the locus (15); and, furthermore, because of the relation (15), the sheet and the plane meet tangentially along this line. Thus the entire line of this intersection maps into the single point $(4\pi R^2,4\pi R^3/3)$ in the (A,V) plane.

Many-sphere multiplets are a special case of Eq. (12) but require special treatment, since A_i and V_i are related. For $M=2$, the partition of area and volume is completely determined by the constraints (13), and there is a unique solution (up to an overall interchange $1\leftrightarrow 2$) provided that $\Delta\le 2^{1/3}-1$, where Δ is the fractional excess (total) area defined by $A=4\pi R_V^2(1+\Delta)$. Since the (σ,p) lines representing the two spheres always cross, they may be regarded as satisfying the coexistence condition with

$$\sigma=(1/R_1+1/R_2)-\tfrac{1}{2},\quad p=2/R_1R_2. \tag{19}$$

When $M\ge 3$, the condition of stationariness $\partial(E+\lambda_A A-\lambda_V V)/\partial R_i=0$ results in a quadratic equation for the multiplet radii, so the conclusion is that the spheres belonging to a multiplet can have at most two different radii. Such states are always local minima with respect to

changes of the radii, since the derivative of Eq. (18) is positive. When $V \gg 1$ and Δ is not too large, then the lowest-energy sphere multiplet always uses one large sphere and $n = 1,2,3,\ldots$ small ones. Representative sphere-multiplet energy diagrams are shown in Fig. 4 for fixed volumes $V = 272$ and 2723. Near $\Delta = 0$ there exist other nonmultiplet configurations of lower energy; however, these multiplets provide one route whereby the original sphere can lower its energy as its area is increased. We shall discuss in Secs. V and VI the extent to which, starting from large initial volumes, this route is actually followed. Note that, when it is, the transitions are first order. When V is sufficiently large, there are no gaps early in this process; for $V \lesssim 420$ a gap first occurs between $n = 1$ and 2, so other configurations are necessarily required.[38]

Properties (b) and (c) (Sec. III) give some further insights. For spheres of the equal radius, the kissing condition (c) can only be satisfied when $R_i = R_0 = 2$ (Helfrich spheres), i.e., along the line $p = \sigma$. Sphere-multiplet configurations ($n \geq 2$) near this line are always close in energy to multiplets including one or more dumbbells (or multiple dumbbells) consisting essentially of Helfrich spheres connected through narrow necks. It follows immediately from Eq. (16) that (for $p < \frac{1}{2}$) $C < 0$ to the right of $p = \sigma$ and $C > 0$ to the left. Thus the stable (i.e., low-energy) configuration will be dumbbells to the right and sphere multiplets to the left. Similarly, for spheres of unequal radius, the kissing condition is satisfied when $\sigma = \frac{1}{2}$ (and $p < \frac{1}{2}$). Near this line, we expect competition from asymmetric dumbbell shapes (or multiple dumbbells involving alternate sizes). The asymmetric necks are stable for $\sigma > \frac{1}{2}$ and the multiplets for $\sigma < \frac{1}{2}$. These special points are indicated in Fig. 4 and will play an important role in later discussion. Note that the $\sigma = \frac{1}{2}$ point is only relevant (i.e., low energy) for the smallest multiplet configuration (S+s). On the other hand, for V sufficiently large the $p = \sigma$ points remain lowest-energy configurations for most higher multiplets (S+ns), as we shall see in Sec. VI.

Nearly spherical shapes can be treated perturbatively,[39–41] provided that the fractional excess area Δ is not too large. For axisymmetric shapes S, we may expand in spherical coordinates in terms of the $m = 0$ spherical harmonics,

$$R(\theta) = R\left[1 + \sum_{l=1}^{\infty} a_l Y_{l,0}(\theta)\right] . \tag{20}$$

The functionals $E[S]$, $V[S]$, $A[S]$, and $\Phi[S]$ all become functions of the distance R and the coefficients $\{a_l\}$. Because of the Euclidean invariance,[42] there is no loss of generality in setting $a_1 = 0$. Thus, for example,

$$\Phi(R,\{a_l\}) - \Phi_0(R) = \sum_{l=2}^{\infty} C_l^{(2)}(R) a_l^2 + \sum_{l_1,l_2,l_3}^{\infty} C_{l_1,l_2,l_3}^{(3)}(R) a_{l_1} a_{l_2} a_{l_3} + \cdots , \tag{21}$$

with

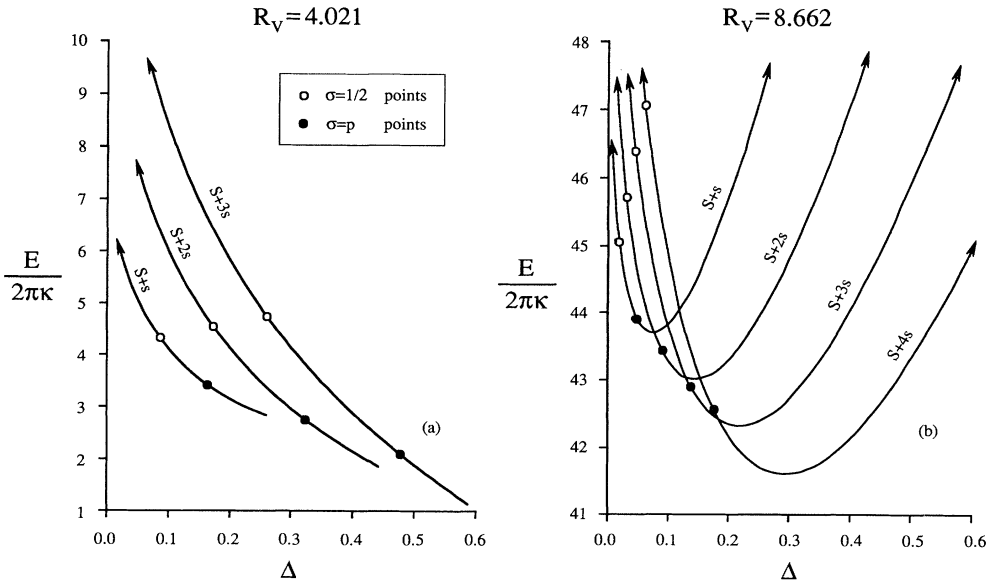

FIG. 4. Curves of energy vs fractional excess area [$A = 4\pi R_V^2(1+\Delta)$] for many-sphere multiplets (S+ns) of fixed volume. The largest possible area of (S+ns) occurs when all spheres have the same radius, i.e., at $\Delta = (n+1)^{1/3} - 1$, independent of R_V. Two representative cases are shown. (a) For small volume ($R_V = 4.02$), the curves do not intersect, and continuity of the energy requires additional phases. (b) For larger volume ($R_V = 8.66$), successive curves intersect (additional phases are required here but for more subtle reasons). At the special points $\sigma = p$ and $\sigma = \frac{1}{2}$, spheres in the multiplet satisfy the kissing condition. Note that the $\sigma = \frac{1}{2}$ point is only relevant (i.e., lowest energy) for the first multiplet. At the larger volume, the $\sigma = p$ points become irrelevant for higher multiplets.

$$C_l^{(2)}(R)=\left[\tfrac{1}{2}(l-1)l(l+1)(l+2)-Rl(l+1)\right.$$
$$\left.+R^2(\tfrac{1}{2}+\sigma)\left[1+\frac{l(l+1)}{2}\right]-pR^3\right]. \quad (22)$$

Terms of order a^3 and a^4 are given in the Appendix. The stationariness of $\Phi[S]$ with respect to R and $\{a_l\}$ leads to a set of nonlinear equations equivalent to Eq. (3). We make use of the fact that these equations have solutions which are perturbative about the spherical shape in powers of $\Delta^{1/2}$, i.e., in which the shape S bifurcates continuously from the sphere. At lowest order, the condition $\partial\Phi_0/\partial R=0$ reproduces Eq. (15) and $\partial\Phi/\partial a_l=2C_l^{(2)}(R)a_l+\cdots=0$ shows that there is a family of such solutions, each dominated by a particular l in the limit $\Delta\to 0$. The locus of the bifurcation in (σ,p) is given by $C_l^{(2)}(R)=0$, which leads to the parametric expression[41]

$$\sigma=\sigma_l=-\tfrac{1}{2}+2/R-l(l+1)/R^2,$$
$$p=p_l=-2[l(l+1)-R]/R^3, \quad (23)$$

as illustrated in Fig. 3. A free-energy sheet corresponding to appropriately deformed quasispherical shapes separates smoothly from the lower sphere sheet along each of these boundaries, as illustrated schematically in Fig. 5. The $l=2$ sheet provides the lowest-energy shape when the fractional excess area (Δ) is small. Expansion near the bifurcation takes the form[43]

$$R=R_V[1-\Delta/2+O(\Delta^{3/2})],$$
$$a_{2n+1}=0,\quad a_2=\sqrt{2\pi}\Delta^{1/2}+O(\Delta),\quad a_{2n}=O(\Delta^{n/2}). \quad (24)$$

The energy of this shape is given by

$$[E(\Delta,R_V)-E_0(R_V)]/2\pi$$
$$=(R_V^2-4R_V+12)\Delta+O(\Delta^{3/2}), \quad (25)$$

which shows how the energy increases as the area increases at constant volume. Terms through $O(\Delta^2)$ are given in the Appendix and will be needed in Sec. VI.

V. SHAPE EVOLUTION AT $V=272$: NUMERICAL RESULTS

To set the stage for a more general discussion of the shape evolution at a large (fixed) volume as area $A=4\pi R_V^2(1+\Delta)$ increases away from the sphere, we present in this section results for a volume $V=272.45$, i.e., $R_V=4.0216$ (in units such that $c_0=1$). The shape calculations on which these results are based were performed using a technique due to Peterson,[39] in which Eqs. (3) and (4) are replaced by five first-order nonlinear equations which handle the singular points [see Eqs. (7) and (8)] in an efficient manner. These equations were integrated by Runge-Kutta methods. They become rather unstable for large volumes,[24] and the choice in our example represents a volume that is appreciably larger than unity but still in a domain where numerical convergence is excellent and details of neck shape can be studied reliably.

Figures 6 and 7 illustrate the shape evolution, including both the energy $E(\Delta)$ and sketches of the corresponding minimizing shapes. Although the energy is continuous as a function of Δ, the curve consists of many segments and is certainly not convex. Each segment corresponds to a region or "phase" in which the shape evolves smoothly. The segments are separated by phase transitions. Both first-order transitions (slope discontinuity) and second-order phase transitions (no-slope discontinuity) are represented. The initial ($\Delta=0$) spherical shape (S) immediately passes through the $l=2$ threshold (Sec. IV) into a prolate elliptical shape (E), which persists until fractional excess area $\Delta=0.070$. At this point (see inset on Fig. 6, point 1) there is a first-order budding transition (in which up-down symmetry is broken) to a necked phase (N) with small neck radius ($a=0.030$, in units such that $c_0=1$). As Δ is increased further, the neck radius shrinks smoothly to zero at $\Delta=0.086$, where there is a second-order transition (point 2) to a multiplet (S+s) consisting of one large sphere ($R=3.97$) plus one sphere

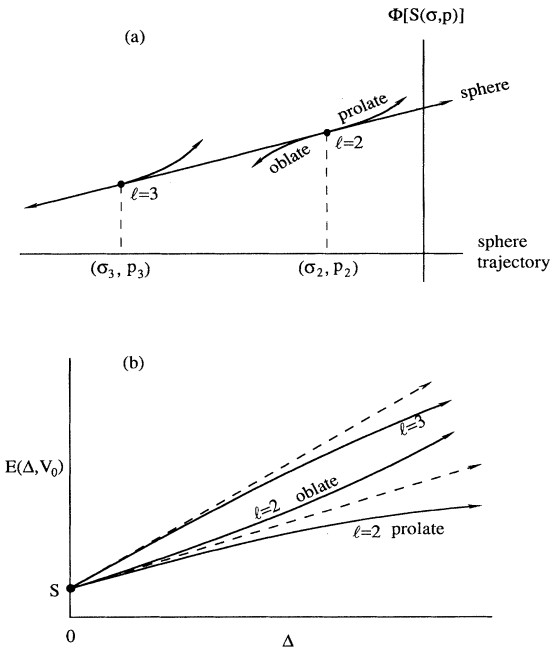

FIG. 5. Structure of bifurcations from the sphere. (a) Sketch of the free energy $\Phi(\sigma,p)$ along a straight line in the (σ,p) plane corresponding to a sphere of fixed radius R, showing bifurcation of the $l=2$ and 3 sheets away from the sphere sheet. Separations between sheets go as $|\sigma-\sigma_2|^3$ and $|\sigma-\sigma_3|^2$, respectively. Note, also, that the $l=3$ bifurcation is one sided. Both these features reflect the up-down symmetry of the problem, which translates in this context into the fact that $\Phi(R,\{a_l\})$ is invariant under simultaneous sign change of all odd coefficients $\{a_{2n+1}\}$. (b) The same structure in the (A,V) plane, showing how the two bifurcations now coincide. The lowest-energy sheet near $\Delta=0$ is always the prolate branch of the $l=2$ shape. The dashed line is the linear approximation, deviations from which go as $\Delta^{3/2}$ and Δ^2 for $l=2$ and 3, respectively.

with a radius ($R=1.34$) somewhat smaller than the Helfrich sphere. On further increase of the area, the smaller sphere grows at the expense of the larger one, until at $\Delta=0.260$ the two spheres have equal volume. At this point (3), one of the two spheres[44] deforms continuously into an elliptical shape, having a volume which grows with Δ, and the remaining sphere starts to shrink (E+s). The transition (S+s)→(E+s) involves a discontinuous jump in the (σ,p) plane and is first order, despite the fact that the actual shape changes are continuous. The (E+s) energy curve crosses the (S+2s) energy curve at $\Delta=0.2866$; however, in this region the (S+2s) multiplet is unstable to another multiplet ($S+d_2$), in which a large sphere coexists with a small symmetric dumbbell. Thus the actual transition is (E+s)→($S+d_2$) at $\Delta=0.2857$ (first order, point 4), followed by ($S+d_2$)→(S+2s) at $\Delta=0.327$ (second order, point 5) on the $p=\sigma$ line, where the neck of the dumbbell shrinks to zero. This scenario appears to continue, with (S+2s)→(E+2s)→($S+d_3$)→(S+3s)→..., where d_3 represents a three-component symmetric dumbbell. The only uncertainty is whether at some stage the $p=\sigma$ point moves far enough to the left so that the transition (E+ns)→(S+(n+1)s) takes place directly. Of course, other shapes presumably appear at sufficiently large Δ; we have only followed the process through $\Delta=0.5$.

The trajectory of the shape evolution in the (σ,p) plane is shown in Fig. 8. Second-order transitions (solid circles) are continuous in this representation; however, first-order transitions involve a discontinuous jump, so each open circle appears twice and there would be corresponding tie lines on the full (σ,p) phase diagram. The bifurcation lines $\sigma=\frac{1}{2}$ and $p=\sigma$ are shown for convenience, along with the $l=2$ threshold (see Sec. IV) and the boundary, Eq. (17), of the allowed-sphere regions. Note, in particular, the mechanism for the (S+s)→(E+s) transition: The (S+s) phase ends at the boundary of the allowed-sphere region, where the radii of the two spheres are equal at $R_1=R_2=R_A/\sqrt{2}$. The phase point then jumps along the (σ,p) line representing a sphere of this radius to its intersection with the $l=2$ threshold. This explains how the transition can be first order but still have a smooth shape variation.

We close this section with a remark on rigor. The Euler equations are nonlinear and have many solutions. It is not hard to follow a particular solution numerically as σ and p are varied; however, there is no general method for proving whether or not the branch one is following has the lowest energy. The existence of multiplet regions makes this problem even more acute, since, in principle, one must test all possible multiplet combinations to search for the lowest energy. We cannot claim to have done this in any rigorous manner. The phase diagrams shown in Secs. V and VI are the result of a search

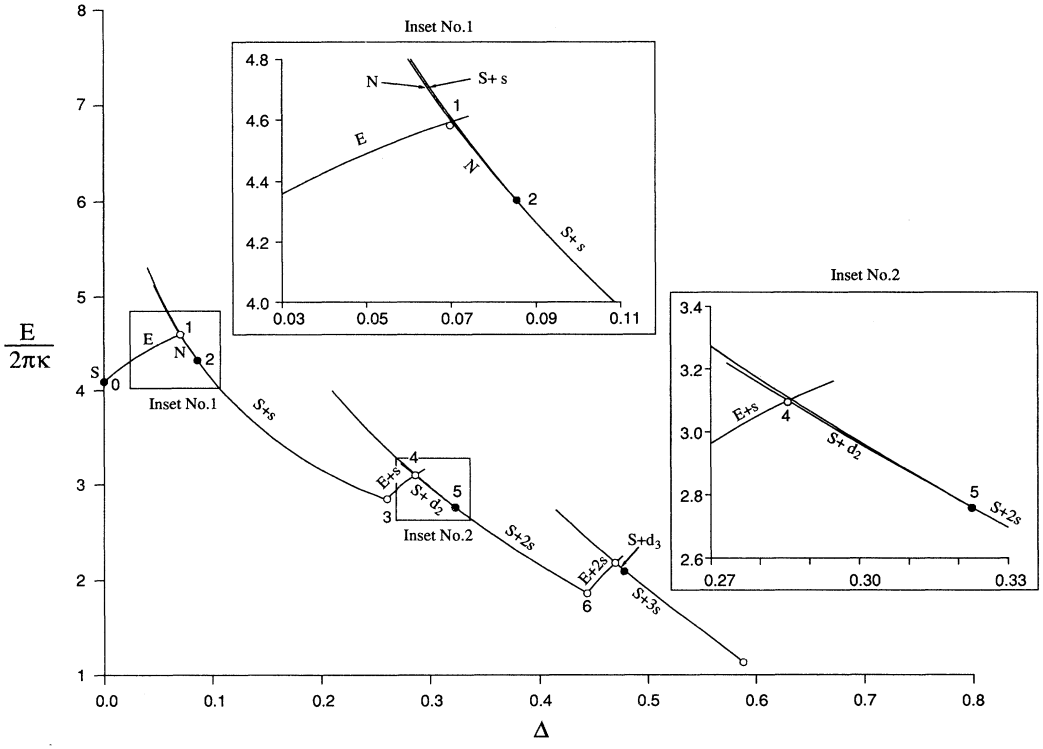

FIG. 6. Energy vs fractional excess area for $R_V=4.02$ ($V=272$). The successive phases (S)→(E)→(N)→(S+s)→ ··· are explained in Fig. 7. Insets show extra detail in special regions. The sequence from (S+2s) through (S+3s) parallels that of (S+s) through (S+2s), shown in the inset. Phase boundary points are labeled S,1,2, ... and appear again in the (σ,p) plane, Fig. 8. First-order transition points (slope discontinuity) are shown as open circles; second-order points (no slope discontinuity, bifurcations) are shown as solid circles. The data are partially analytic and partially from numerical solution of the Euler equation.

only over those configurations, singlet and multiplet, which we have found and considered likely candidates.

VI. ANALYTICAL RESULTS FOR THE PHASE DIAGRAM AT LARGE VOLUME

To find the full phase diagram, one may repeat the calculations of Sec. V for many different volumes and simply tabulate the results. A rather complete study of this sort has recently been carried out by Seifert, Berndl, and Lipowsky[14] for a range of $R_A, R_V \sim 1$ (in our units). On the other hand, as we shall outline in this section, at large volumes and fractional excess areas which are not too large, the phase boundaries may be mapped out quasi-analytically. In this region the numerical integrations become unstable, and, in this sense, our work complements that of Seifert, Berndl, and Lipowsky, extending it to large volumes, where budding and vesiculation dominate the phase diagram.[45]

Conceptually, the scenario is as anticipated in Sec. IV: A sphere of volume NV_H with $N \gg 1$ ($V_H = 32\pi/3$ is the volume of the Helfrich sphere) vesiculates off a sequence of small spheres, as its area is increased. As long as $A \ll NA_H$ (where $A_H = 16\pi$ is the area of the Helfrich sphere), the minimum-energy configuration is always a multiplet which consists in effect of n ($\ll N$) Helfrich spheres (which cost no energy) and one larger sphere, which carries the remaining volume. As area increases, the energy decreases from $E = 8\pi(N^{1/3} - 1)$ at $A = 4\pi R_V^2$ to near zero at $A = NA_H$ ($E = 0$ when N is an integer).

These successive vesiculations are essentially periodic in A with period A_H, as each increment of area is shed in the form of a Helfrich sphere. Between successive vesiculations, the additional area can be absorbed either by increasing the radius of the small spheres at the expense of the large one or by deforming the large sphere (which, it turns out, always costs less energy than deforming the small ones). The former route is always preferable when it is possible; but, as we shall see below, it is not always possible at low volume. The vesiculation $(n-1) \rightarrow n$ normally occurs when the radius of the n small spheres is slightly less than R_0, i.e., at a point just to the right of the line $\sigma = p$, where, as discussed in Sec. IV, $C < 0$ and n independent small spheres always have higher energy than an n-fold multiple dumbbell (d_n) of the same volume[46] (see Fig. 9). Whenever this is true, the dumbbell phase ($S + d_n$) precedes the phase ($S + ns$) in the vesiculation sequence. The scenario sketched above holds until n becomes comparable to N. For $n \gtrsim N$ (large area A), E must begin to increase with A, it becomes energetically preferable to use nonspherical shapes in the multiplets.

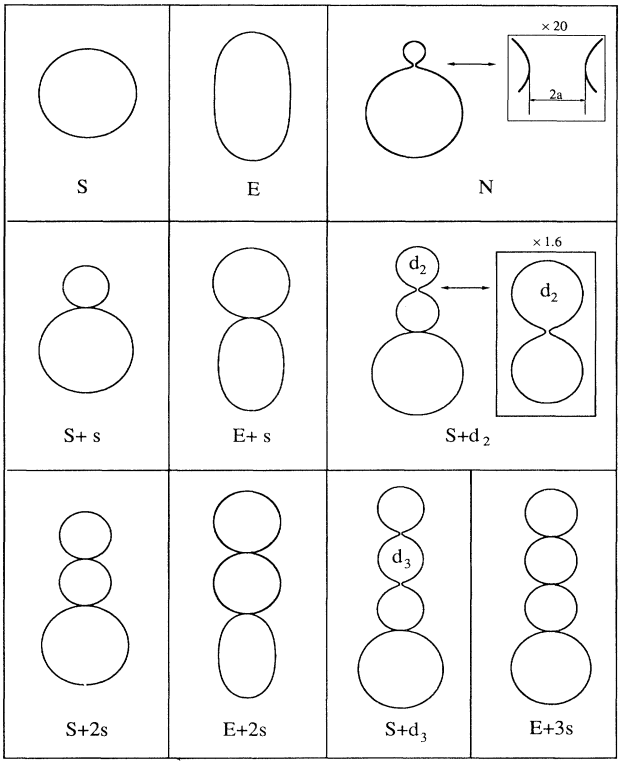

FIG. 7. Vesicle shapes corresponding sequentially to the different regions (phases) of Fig. 6 ($R_V = 4.02$). S represents sphere; E, "ellipse"; N, neck; S+s, two-sphere multiplet; E+s, "ellipse" plus sphere multiplet; S+d_2, sphere plus two-part dumbbell; etc. The figures are drawn properly to scale, except that it has been necessary to exaggerate the width of narrow necks to make them visible at this magnification.

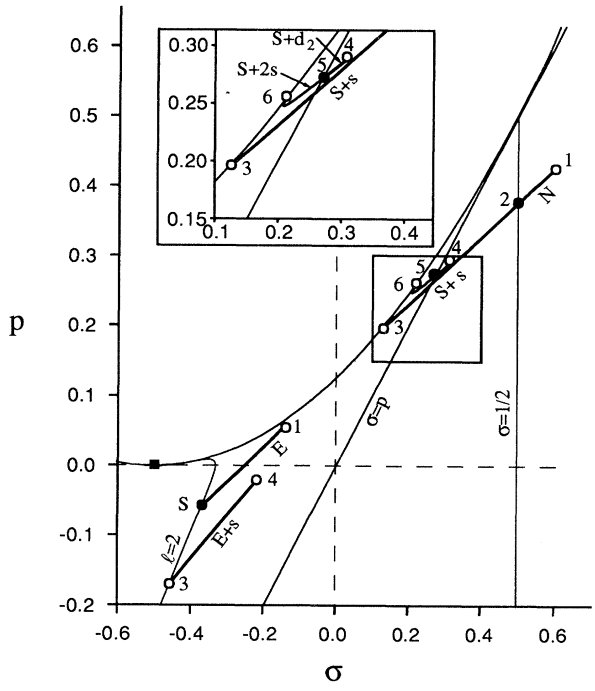

FIG. 8. The trajectory of area expansion at constant volume ($R_V = 4.02$) traced out in the (σ, p) plane. Notation corresponds to that of Figs. 6 and 7. Note that the phase point jumps discontinuously at first-order transitions, so that, e.g., the point 1 [(E)→(N)] appears twice. Second-order transitions occur at bifurcation lines (here, $l = 2$, $\sigma = p$, and $\sigma = \frac{1}{2}$, shown as thin lines). Inset shows detail.

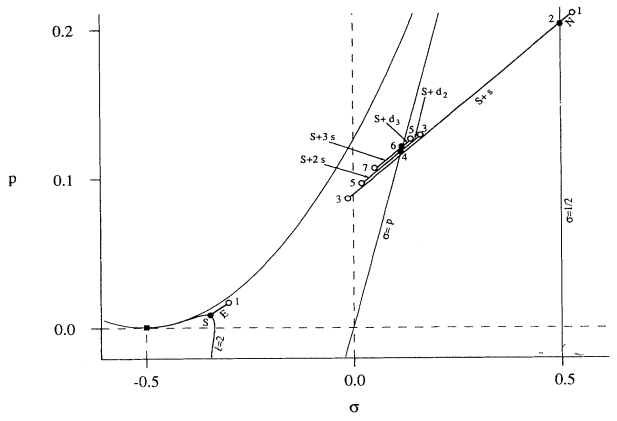

FIG. 9. Same as Fig. 8 but for the larger volume $R_V=8.66$ ($V=2723$). Note here that, in contrast to Fig. 8, the multiplet phase (S+s) becomes unstable to (S+d_2) before reaching the parabolic ("no-sphere") boundary. (S+d_2) transforms to (S+2s) at a second-order transition, when it reaches the bifurcation line $\sigma=p$. For nonspherical shapes the data are approximate, based on perturbative results. Separations between multiplet trajectories are exaggerated by about a factor of 2 in order to make the sequence structure visible at this scale.

and other configurations may occur. This large-area, large-volume region of the phase diagram remains to be explored.

Figure 10 shows the large-volume phase diagram and includes data through the fourth vesiculation. The lowest volume shown corresponds to $V=2V_H$ ($R_V=2^{4/3}$), which is the minimum volume at which the first vesiculation can take place via the mechanism we have described, since the $\sigma=\frac{1}{2}$ bifurcation line (Fig. 4) ends at $p=\frac{1}{2}$, where the corresponding radius is that of the Helfrich sphere. Volumes comparable to and smaller than this have been explored in Ref. 14.[47] More generally, when $R_V/R_0\sim n^{1/3}$, new phases and new phase sequences—not shown in Fig. 10—can and do occur. Generally, the (S+($n-1$)s) phase does not occur below the point labeled H_n [$\Delta=n^{1/3}-1, R_V=2(n)^{1/3}$], where n Helfrich spheres coexist.

The sequence of phases, as Δ increases at fixed V, is similar to what we observed in Sec. V, but with some important modifications:

(a) One difference is the absence above appropriate critical volumes of the (E+ns) phases, which in Sec. V intervened between (S+ns) and (S+d_n) in the sequence (S+ns)$\rightarrow\cdots\rightarrow$(S+($n+1$)s). The reason for this—already anticipated in Fig. 4—is that the energy curves

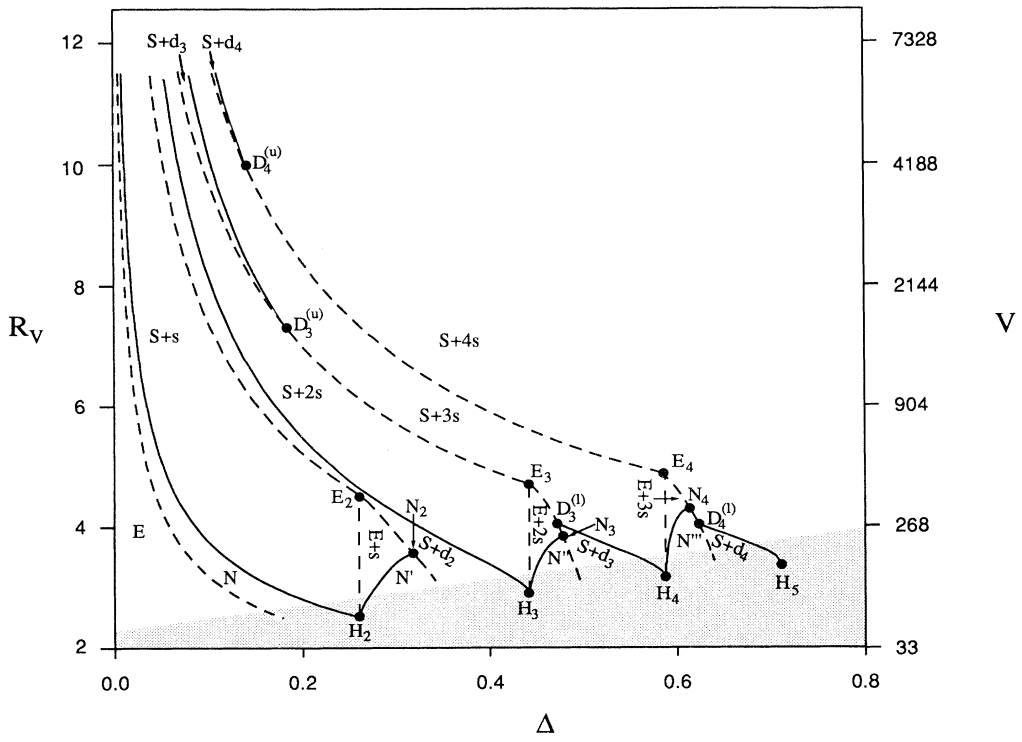

FIG. 10. Phase diagram for the Helfrich curvature model in the region of large volume ($V=4\pi R_V^3/3$) and small excess area [$A=4\pi R_V^2(1+\Delta)$]. The labeling of the phases is given in Fig. 7, except for (N'), (N''), etc., which are discussed in the text. First-order transitions are shown by dashed lines; second-order transitions, by solid lines. The location of special points is provided in Table I. The gray region corresponds to $\Delta\gtrsim(R_V/2)-1$ (i.e., areas comparable to and larger than N Helfrich spheres), where the phase diagram is not controlled by the arguments given here. The phase diagram in this region may be found in Ref. 14, if Δ is not too large. At high area, the phase diagram is not yet known, and it is probable that nonaxisymmetric phases play a role.

$E_{S+ns}(\Delta)$ overlap at sufficiently high volume, and the small-sphere (s) members of the multiplets remain on the scale of the Helfrich sphere. In Fig. 10 we have denoted by E_{n+1} the largest-volume point of the phase (E+ns).

(b) Another difference is the disappearance of the dumbbell phase (S+d_n) at intermediate volumes for $n \geq 3$. The mechanism for this disappearance is the movement of the $p=\sigma$ point into an unphysical (i.e., high-energy) region over this interval. The corresponding lower and upper boundaries of the (S+d_n) phase we denote $D_n^{(l)}$ and $D_n^{(u)}$, respectively.

(c) Finally, at volumes near but above $(n+1)V_H$, the (E+ns) phase crosses the (E)-(s) kissing boundary,[48] as area increases, before becoming unstable to (S+d_{n+1}). At this boundary, the coefficient C describing the axial E↔s neck changes sign, so it becomes energetically favorable to open up nonzero necks, resulting in the phases (N′), (N″), etc.[49] Thus (N′) has the same symmetry as (N) (and may, perhaps, be connected to it below H_2). (N″) has the form s-E-s connected through nonzero necks. The structure of (N‴) is less clear; but (s-E-s+s) (a multiplet) seems likely, at least close to the phase boundary. The largest-volume points of these new necked phases are designated N_2, N_3, etc.

Positions of the special points H_n, E_n, $D_n^{(l)}$, $D_n^{(u)}$, and N_n are given in Table I.

We turn now to the location of the phase boundaries. The necking boundary, (E)↔(N), is first order and must in principle be calculated numerically. However, the energy curves for the (N) and (S+s) phases lie very close by, as is already visible in Fig. 6, so an excellent approximation can be obtained simply by equating the perturbative expression (25) (including the higher-order corrections [Eq. (A4)]) to the energy of the (S+s) multiplet.[50] At high volume the fractional excess area at the transition is $\Delta_1 = 1/R_V^2 + O(1/R_V^3)$. The (second-order) vesiculation boundary (N)↔(S+s) is just the $\sigma=\frac{1}{2}$ curve, $R_V = 1/r_1(\Delta) + 1/r_2(\Delta)$ with $r_1^3 + r_2^3 = 1$ and $r_1^2 + r_2^2 = 1+\Delta$. The range of Δ over which the necked phase (N) exists decreases in width at high volume like (const)$/R_V^4$.[51] The boundary between (S+ns) and (E+ns) occurs when the radius of the n small spheres has grown to that of the coexisting large sphere, i.e., along the sphere boundary (17), which gives $\Delta = (n+1)^{1/3} - 1$, independent of volume. (E+ns)↔(S+d_{n+1}) is first-order [like (E)↔(N)] but, again, because the dumbbell neck energy is small, it is well approximated by equating the (E+ns) energy (numerical or perturbative) to the (S+(n+1)s) energy (analytic). The boundary (E+ns) ↔($N^{n'}$) requires knowing the volume and axial curvature of the "ellipse" shapes, both of which can be well approximated perturbatively, giving the curves shown. Finally, the second-order vesiculation boundary (S+d_n)↔(S+ns) is the $\sigma=p$ curve, $R_V = 2/r_2(\Delta)$ with $r_1^3 + r_2^3 = 1$ and $r_1^2 + n r_2^2 = 1+\Delta$.

TABLE I. Location of special points in the phase diagram (Fig. 10). H_n corresponds to a multiplet of n coexisting Helfrich spheres ($R=2$). E_{n+1} are the points above which the phase (E+ns) does not occur. $D_n^{(u)/(l)}$ are the points above/below which the dumbbell phase (S+d_n) occurs. N_n are the points below which the neck phases (N′), (N″), etc. are found. Where analytical expressions are not shown, the coordinates rely on numerical results and/or perturbative expressions, and corresponding uncertainties are given.

	Δ	R_V
H_2	$2^{1/3}-1=0.260$	$2\times 2^{1/3}=2.520$
H_3	$3^{1/3}-1=0.442$	$2\times 3^{1/3}=2.884$
H_4	$4^{1/3}-1=0.587$	$2\times 4^{1/3}=3.175$
E_2	0.260±0.005	4.65±0.02
E_3	$3^{1/3}-1=0.422$	4.71±0.01
E_4	$4^{1/3}-1=0.587$	4.91±0.01
$D_3^{(u)}$	0.187±0.005	7.22±0.05
$D_4^{(u)}$	0.140±0.005	9.95±0.05
$D_3^{(l)}$	0.472±0.003	4.06±0.02
$D_4^{(l)}$	0.623±0.005	4.04±0.02
N_2	0.318±0.005	3.52±0.05
N_3	0.476±0.005	3.92±0.05
N_4	0.613±0.005	4.30±0.05

VII. CONCLUDING REMARKS

The results of this paper combined with those of Seifert, Berndl, and Lipowski[14] for the low-volume regime give now for the first time a good idea of the shape phase diagram for the axisymmetric Helfrich model (1). The only region not yet mapped out is the region of high area and high volume, $R_A^2/R_V^2 = (1+\Delta) \gtrsim R_V/R_0 \gg 1$. It will not be an easy task to treat this region, since numerical stability will be a problem and multiplet configurations involving nonspherical Euler shapes will have to be considered.

How much will the inclusion of nonaxisymmetric shapes change the general scenario developed here for shape evolution driven by area increase at fixed volume? We are not in a position to answer this important question firmly; however, we argue that likely modifications are minor. Observe, first, that the energy functional (1) is non-negative, so the basic mechanism of shedding area into shapes that are essentially Helfrich spheres seems very robust. As long as the degree n of vesiculation is small relative to $N \equiv V/V_H$, relevant configurations will be multiplets consisting of one large Euler shape (S, N, or E in what we have studied) and, effectively, n smaller Euler shapes on the scale of R_0. The issue of stability is then equivalent to asking whether or not these shapes can be reduced in energy by nonaxisymmetric changes which preserve volume and area. It is already clear from Eq. (25) that spheres are locally stable to axisymmetric perturbations which increase area at fixed volume. Instability might arise if spheres (S) or ellipses (E) were energetically unstable to nonaxisymmetric shapes; however, Peterson[39] has studied this question and apparently verified local stability for all the shapes relevant to us. This leaves only two problematic shapes, (N) and the various dumbbells (d_n). Stability of the necked Euler

shapes has not been studied. Note, however, that our phase diagram uses shapes (N) with neck radii always much less than R_0, so it seems likely that any significant modification must occur in the neck region. While we cannot rule out nonaxisymmetric modification of the neck shape, any such change would have to occur at a length scale small with respect to R_0, which seems unlikely. The dumbbells, on the other hand, are a different story. These shapes are basically Helfrich spheres fused through narrow necks; but, there seems no special reason to suppose that the linear configuration forced by the assumption of axisymmetry should have the lowest possible energy at fixed area and total (dumbbell) volume. The condition that the system remain topologically spherical limits the number of necks to $n-1$; however, the energetic interactions between the necks may well prefer a nonaxisymmetric "branching" pattern of the connected spheres. Thus, our best guess is that, for $n \ll N$, extending consideration to nonaxisymmetric shapes will not change Fig. 10 significantly, except possibly to replace the linear dumbbells d_n by some more exotically branched shape. On the other hand, in the large-volume and large-area regime referred to in the preceding paragraph, none of these arguments apply, and significant breakdown of axisymmetry may well be the rule rather than the exception.

If a "real" system were found to which the Helfrich model applied (as we have formulated it, with fixed spontaneous curvature c_0), one might still ask whether the behavior predicted here would be observed in an experiment which scanned across the phase diagram. At issue are questions of dynamics and metastability: Will one minimum-energy shape evolve from another, as, e.g., area is increased at constant total volume? We mention two examples to illustrate possible effects.

Consider first the "necking" transition (E)→(N). This phase boundary is first order, and metastability is expected. In particular, Peterson's analysis[39] shows that the shape E is locally stable at the transition; thus, in an experiment, the vesicle would follow the energy curve $E_E(\Delta)$ beyond the transition and on up in area to within an energy k_BT of the first instability (Δ_c). At this point, the vesicle would "fall" down a trajectory which depended on dynamical considerations to the lowest energy configuration at the area corresponding to Δ_c.[52] Such a transition would not be reversible, and hysteresis would result.

Another problem is dynamical blocking. The simplest example here is the evolution of the multiplet shapes. In order for these shapes to adjust as area changes, matter must be able to flow through the zero-radius necks which still join the members of the multiplet on experimental time scales. Of course, in the laboratory such necks will have some nonzero radius determined by whatever natural length fixes the short-distance cutoff of applicability of the simple Helfrich model. One might expect such a radius to be of the order of, say, 20 Å for simple lipid-bilayer systems. Fluid flow through such a narrow aperture can be slow.

Although our work was motivated by experiments,[12,17–19] it is far from clear that the model we have studied is an appropriate description of what is seen in the laboratory. Chemical mechanisms[10] have difficulty accounting for a spontaneous curvature which is large enough to explain the micrometer-scale buds which are observed. The bilayer-couple mechanism of Svetina and co-workers[11] is an attractive hypothesis. This approach uses an energy functional which differs from our Eq. (1) in lacking the c_0 term and, thus, leads to a different phase diagram and different shape sequences, even though the free-energy surfaces are the same. This model has recently been tested[18] in the low-volume regime, where it is able to explain the sequences observed in Sackmann's laboratory. On the other hand, it predicts that the (E)→(N) transition is second order rather than first order (as we find it), which appears to be in disagreement with the observations of Evans and Rawicz.[12]

Another worrying inconsistency surrounds the formation of tubules. These structures have internal radii of 15–20 Å and appear frequently but not always in experiments.[12] Such tubular forms can be found as Euler shapes in the Helfrich problem[53] and may occur as a result of mechanically drawing out a cylindrical tether.[54] However, there is no evidence whatsoever that they are low-energy structures in the regime where budding and vesiculation are observed. It is possible that such shapes would appear naturally in the minimization problem if short-distance effects, neglected in the Helfrich model, were included (van der Waals attraction, higher-order curvature terms, etc.). Indeed, Bruinsma[55] has recently shown how van der Waals interactions may stabilize tubular structures and/or cause dynamical instability towards beadlike structures, which, under appropriate circumstances, might resemble our equilibrium multiplets.

ACKNOWLEDGMENTS

We acknowledge with pleasure useful conversations with R. Grebe, W. Helfrich, B. Klösgen, S. Leibler, R. Lipowsky, E. Sackmann, U. Seifert, and M. Zuckermann. We are grateful to W. Helfrich, R. Lipowsky, and U. Seifert for sending copies of their work prior to publication and to U. Seifert for a careful reading of our manuscript. We thank our collaborator E. Evans for his wisdom and encouragement, for his unfailing enthusiasm, and for introducing us in his laboratory to the intricacy of fluid-membrane preparation and behavior. This work was funded in part by the Natural Sciences and Engineering Research Council of Canada and by the U.S. National Science Foundation through the Division of Materials Research.

APPENDIX: PERTURBATIONS FROM THE SPHERE

We collect here expressions for the higher-order corrections referred to in Sec. IV. Extending Eq. (21), we find

$$C^{(3)}_{l_1,l_2,l_3}(R)=\frac{G(l_1,l_2,l_3)}{3}\left[\frac{(R+2)}{2}[l_1(l_1+1)+l_2(l_2+1)+l_3(l_3+1)]\right.$$
$$-\frac{R}{2}[l_1(l_1+1)l_2(l_2+1)+l_2(l_2+1)l_3(l_3+1)+l_3(l_3+1)l_1(l_1+1)]$$
$$\left.+\frac{(R-2)}{4}[l_1^2(l_1+1)^2+l_2^2(l_2+1)^2+l_3^2(l_3+1)^2]-pR^3\right], \tag{A1}$$

where

$$G(l_1,l_2,l_3)=\int d\Omega\, Y^0_{l_1}(\Omega)Y^0_{l_2}(\Omega)Y^0_{l_3}(\Omega)\,, \tag{A2}$$

which is easily expressed in terms of Clebsch-Gordan coefficients and vanishes unless triangle inequalities and parity are satisfied. The fourth-order term in Eq. (21) is even more cumbersome. For our purposes it suffices to give only the term in a_2^4, which is required in extending Eq. (25),

$$\Phi^{(4)}(R,a_2)=\frac{15}{56\pi}[-3(1+2\sigma)R^2+20R-24]a_2^4\,. \tag{A3}$$

The additional terms which extend Eq. (25) for the bending energy of the "elliptical" ($l=2$) shape are

$$-\frac{4\sqrt{10}}{21}(5R_V+6)\Delta^{3/2}-\frac{(27R_V^2+76R_V+12\,612)}{1029}\Delta^2+O(\Delta^{5/2})\,. \tag{A4}$$

---

*Present address: Institute Laue-Langevain, Avenue des Martyrs, B.P. 156X, 38042 Grenoble CEDEX, France.

[1]B. Alberts, D. Bray, J. Lewis, M. Raff, K. Roberts, and J. D. Watson, *Molecular Biology of the Cell* (Garland, New York, 1983); W. Becker, *The World of the Cell* (Benjamin/Cummings, Reading, MA, 1986).

[2]Good general references are (a) *Statistical Mechanics of Membranes and Surfaces,* edited by D. Nelson, T. Piran, and S. Weinberg (World Scientific, Singapore, 1989), see especially papers by S. Leibler and F. David; (b) *Physics of Amphiphillic Layers,* edited by J. Meunier, D. Langevin, and N. Boccara (Springer-Verlag, Berlin, 1987).

[3]P. B. Canham, J. Theor. Biol. **26**, 61 (1970).

[4]W. Helfrich, Z. Naturforsch. **28c**, 693 (1973).

[5]H. J. Deuling and W. Helfrich, J. Phys. (Paris) **37**, 1335 (1976).

[6]E. Evans and R. Skalak, *Mechanics and Thermodynamics of Biomembranes* (CRC, Boca Raton, FL, 1980); see also, E. A. Evans, Biophys. J. **30**, 265 (1980).

[7]J. T. Jenkins, J. Math. Biol. **4**, 149 (1977).

[8]M. A. Peterson, Mol. Cryst. Liq. Cryst. **127**, 257 (1985).

[9]M. A. Peterson, J. Math. Phys. **26**, 711 (1985).

[10]E. A. Evans, Biophys. J. **14**, 923 (1974).

[11]S. Svetina, A. Ottova-Lietmannová, and R. Glaser, J. Theor. Biol. **94**, 13 (1982); S. Svetina and B. Žekš, Biomed. Biochem. Acta **42**, S86 (1983); **44**, 979 (1985); S. Svetina, M. Brumen, and B. Žekš, Stud. Biophys. **110**, 177 (1985); S. Svetina and B. Žekš, Eur. Biophys. J. **17**, 101 (1989).

[12]Typical values quoted for lecithins are $(0.4–2.0)\times10^{-12}$ ergs or $(10–20)k_BT_{\rm room}$. E. Evans and W. Rawicz, Phys. Rev. Lett. **64**, 2094 (1990).

[13]$c_0<0$ is achieved in this convention by closing the vesicle "inside out," i.e., below $z=0$ in Fig. 1.

[14]U. Seifert, K. Berndl, and R. Lipowsky, Phys. Rev. A (to be published).

[15]The only qualification of this restriction is the careful study of simple axisymmetric shapes against nonaxisymmetric perturbations; see Refs. 39–41.

[16]M. Bessis, *Living Blood Cells and Their Ultrastructure* (Springer-Verlag, Berlin, 1973).

[17]E. Sackmann, H.-P. Duwe, and H. Engelhardt, Faraday Discuss. Chem. Soc. **81**, 281 (1986).

[18]K. Berndl, J. Käs, R. Lipowsky, E. Sackmann, and U. Seifert, Europhys. Lett. **13**, 659 (1990).

[19]W. Harbich and W. Helfrich, Chem. Phys. Lipids (to be published).

[20]A situation which in our context should be interpreted as meaning that a decreases to some physically determined microscopic dimension at which new physics enters the problem, thus providing an ultraviolet cutoff to the curvature Hamiltonian.

[21]J. C. Luke and J. I. Kaplan, Biophys. J. **25**, 107 (1979).

[22]W. Wiese and W. Helfrich, J. Phys. Condens. Matter **2**, SA329 (1990).

[23]Indeed, they seem to think that the vesiculated shapes are always mechanically unstable, so that small necks must open (which, as we shall show, is not true). We have the impression that their algorithm for computing the Euler shapes does not handle narrow necks efficiently.

[24]B. Fourcade, L. Miao, M. Rao, M. Wortis, and R. K. P. Zia (unpublished).

[25]By relating the energetic approach to one based on mechanics (see Ref. 6), these Lagrange multipliers may be related to mechanical quantities. p turns out to be just the pressure difference between the inside and outside of the vesicle, and σ is closely related (but not equal) to the mechanical surface tension.

[26]Note that the rotation invariance of the energy functional $E[S]$ and the constraints guarantees that shapes which satisfy the axial Euler equation are stationary with respect to local nonaxial perturbations. It is not guaranteed, however, that such stationary shapes are local minima, and, indeed, it is not always true. This point has been explored by Peterson, Ou-

Yang, and Helfrich in special cases (Refs. 39–41).

[27]It may be asked at this point why one does not form directly the energy surfaces $E_n(\sigma,p)$ rather that the free-energy surfaces. The answer is that the Legendre-transform structure makes Φ the "natural" free energy. Relations like Eq. (9) and (10) mean that local second-order structure is normally preserved (but see Ref. 28 for an exception).

[28]The exception is the sphere sheets $\Phi_{\text{sphere}}(\sigma,p)$, which transform into a line in $E(A,V)$, thus changing the associated bifurcation structure significantly. We shall discuss this in some detail in Sec. IV. This apparent anomaly is actually a simple consequence of the Euclidean invariance of the problem.

[29]Note that the lowest sheet $E_m(A,V)$ does not necessarily correspond to the lowest sheet $\Phi_n(\sigma,p)$ at the corresponding values $\sigma(A,V)$ and $p(A,V)$.

[30]The continuity of $E(A,V)$ can presumably be proved rigorously by arguing that a shape S, which has energy E at area A and volume V, can always be slightly modified in such a way as to acquire area $A+\delta A$ and volume $V+\delta V$ with an energy change δE which goes to zero as δA and δV go to zero.

[31]If fission occurs, then the omitted Gaussian curvature terms would have to be put in.

[32]This corresponds in unnormalized units to $2/R_0-1/R_1-1/R_2$, where R_0 is the spontaneous radius of curvature.

[33]We have assumed here that A_i and V_i are independent variables. This is true for all Euler shapes except spheres, which require special treatment, since the spherical radius R_i determines both A_i and V_i. We shall comment further in Sec. IV. The conclusion is that this result holds equally for spheres.

[34]An example here is the situation for spheres, which we shall study in detail in Sec. IV. Of course, in the spherical case A and V are not independent and the relevant condition is $\partial^2 E/\partial R^2>0$.

[35]An example of this is elliptical shapes which are not too far from spheres, for which $\partial^2 E/\partial A^2<0$, as we shall show in Sec. IV.

[36]Note that σ and p are not restricted to be positive. Negative values of R correspond to spheres whose curvature is opposite to the spontaneous curvature c_0, here set to unity.

[37]M. J. Sewell, *Maximum and Minimum Principles* (Cambridge University Press, Cambridge, England, 1987), p. 98ff.

[38]Actually, for reasons discussed in Sec. VI, these other configurations come in slightly before the gap opens.

[39]M. A. Peterson, J. Appl. Phys. **57**, 1739 (1985).

[40]S. T. Milner and S. A. Safran, Phys. Rev. A **36**, 4371 (1987); S. A. Safran, J. Chem. Phys. **78**, 2071 (1983).

[41]Ou-Yang Zhong-can and W. Helfrich, Phys. Rev. Lett. **59**, 2486 (1987); **60**, 1209 (1987); Phys. Rev. A **39**, 5280 (1989).

[42]E, Φ, A, and V are invariant under Euclidean transformations of S. What is important here is that translations of S along the symmetry axis induce nonlinear transformations on the coefficients $\{\alpha_l\}$ but leave the values of these functionals unchanged.

[43]The absence of odd terms is general for even l and follows from the up-down symmetry of the problem.

[44]Note that the two-ellipse multiplet cannot be stable by the argument given in Ref. 35.

[45]These phenomena are observed at the lower volumes of Ref. 14, but they play a less dominant role there.

[46]Since opening necks lowers the energy in this region, one large-multiple dumbbell is always preferable to several smaller ones with the same total volume. Note that the asymmetric dumbbell, based on fusing S and s, is not stable in this region to the left of $\sigma=1/2$.

[47]According to Ref. 14, just below $V=2V_H$ the sequence of phases is reentrant: (E) goes to (N) (called "pear" in Ref. 14) via a first-order transition, but then the neck grows again and, at a higher area, (N) reconverts to (E) by a bifurcation (second order).

[48]We are grateful to U. Seifert for questioning us on this point.

[49]Another possible option might come to mind here: If the ellipse grows in area sufficiently, then it could become unstable to necking (E)→(N). If this happened before the boundary (S+d_n), then it would compete with (N'), (N''), etc., and some other stable phase might intervene. As far as we have been able to tell, this does not happen in the part of the phase diagram we have studied; however, we have no general proof.

[50]The correction terms, already small at $R_V=4$, may be calculated using the methods of Ref. 24.

[51]Interestingly, the value of the constant seems not to be fully determined by the coefficients in the Appendix; however, we believe that the evidence is strong that it is positive and of order unity.

[52]Of course, depending on details of the local energy surface and the frictional (viscous) forces, the system might also end up in another metastable minimum.

[53]H. J. Deuling and W. Helfrich, Blood Cells **3**, 713 (1977).

[54]R. M. Hochmuth, H. C. Wiles, E. A. Evans, and J. T. McCown, Biophys. J. **39**, 83 (1982); R. E. Waugh and R. M. Hochmuth, *ibid.* **52**, 391 (1987); Lin Bo and R. E. Waugh, *ibid.* **55**, 509 (1989).

[55]R. Bruinsma, J. Phys. (Paris) Colloq. **51**, C7-53 (1990).